SEMARAK ILMU PUBLISHING

Semarak International Journal of Material Research

Journal homepage:
https://semarakilmu.my/index.php/sijmr/index
ISSN: 3083-8908

Structural and Mechanical Properties of Zinc-Strontium-Lithium Phosphate Glass Doped with Carboxymethyl Cellulose

Siti Norfariza Farhana Mohd Razak[1], Nur Hazwani Mohd Yusoff[1], Nurhafizah Hasim[1,*], Nur Hidayah Ahmad[1], Norshahirah Mohamad Saidi[1], Mohd Fuad Mohamad[2], Anis Nazihah Mat Daud[3]

[1] Advanced Optical Materials Research Group, Faculty of Science, Universiti Teknologi Malaysia, Johor, Skudai, 81310, Malaysia
[2] Department of Chemistry, Faculty of Science, Universiti Teknologi Malaysia, Johor, Skudai, 81310, Malaysia
[3] Department of Physics, Faculty of Science and Mathematics, Universiti Pendidikan Sultan Idris, 35900 Tanjung Malim, Perak, Malaysia

ARTICLE INFO

Article history:
Received 10 November 2024
Received in revised form 8 December 2024
Accepted 15 December 2024
Available online 30 December 2024

Keywords:
Phosphate glass; FTIR; Raman

ABSTRACT

A series of phosphate glasses doped with carboxymethyl cellulose (CMC) was synthesized using the melt-quenching technique to explore their structural and mechanical properties. The composition (40–x) P_2O_5-ZnO-Li_2O–SrO-xCH_2CO_2H (0.0 ≤ x ≤ 0.5 mol%) was characterized using Fourier Transform Infrared (FTIR) spectroscopy, Raman spectroscopy, ultrasonic testing, and Vickers hardness measurements. Results revealed that the addition of CMC caused subtle structural changes, enhancing the glass network's compactness and stiffness. Mechanical analysis showed improved hardness, elasticity, and self-cleaning properties, making this system a viable candidate for applications in food processing and healthcare, where surface contamination is a concern. This study highlights the potential of biodegradable, non-toxic phosphate glass for innovative and sustainable applications.

1. Introduction

Malaysia is known with their islands and also beaches that are really famous among locals, especially with their variety of seafood that is also very famous with health benefits [14,15]. Fish or other seafood is well known as a source of protein among Malaysians [1]. Because they are probably mistaken for food, these microscopic plastic polymers can be consumed by marine life and build up in their tissues, circulatory systems, and even brains [2]. Therefore, the consumption of fish or other seafood is leading humans to be exposed to the ingestion of microplastics.

The increasing demand for sustainable and multifunctional materials has propelled research into advanced glass systems with unique properties. Among these, phosphate glasses stand out due to their excellent optical, chemical, and mechanical characteristics. Unlike conventional silicate and borate glasses, phosphate glasses are versatile, allowing for doping with various metal oxides to tailor properties for specific applications. Zinc oxide (ZnO), lithium oxide (Li_2O), and strontium oxide (SrO)

* *Corresponding author.*
E-mail address: nurhafizah.h@utm.my

https://doi.org/10.37934/sijmr.1.1.2640 a

are particularly effective modifiers, offering enhanced chemical durability, mechanical strength, and antimicrobial properties, [9;10;11] making phosphate glasses suitable for applications ranging from biomedical devices to optoelectronics.

Carboxymethyl cellulose (CMC), a biopolymer derived from cellulose, is gaining traction as a sustainable additive in material science. Known for its water solubility, biocompatibility, and ease of modification, CMC has been extensively used in packaging, coatings, and composites [12;16]. Its inclusion in glass matrices can improve mechanical strength, crystallinity, and barrier properties. Despite its widespread use, the effect of CMC on phosphate glass, especially its structural and mechanical properties, has not been thoroughly explored.

Phosphate glass performs better than silicate and borate glasses when it comes to combining appropriate glass composition in research setting because it is encouraged in daily life and has the mixing ability and flexibility of shape and size at a relatively low cost [3]. Phosphate glasses differ from other types in that they can be doped with most transition metal oxides [4]. After being combined with phosphate glasses, the zinc oxide and phosphate molecules formed a chain bond. This bond is moisture-resistant [3]. Zinc oxide (ZnO) possesses antimicrobial properties and low toxicity [5].

Lithium phosphate glasses are made from phosphate glasses doped with alkaline oxide like Li_2O [4]. Glasses with lithium added offer numerous benefits, including strength, polaron character, and wide formability, and that is the reason it is used in many applications, like in optoelectronic devices, dental applications, and lithium-ion conducting glasses [6]. Glass made of strontium-modified phosphate (Sr-PBG) is recognized for its ability to provide long-lasting bacterial resistance. One of the many ion species that are liberated from traditional and resin-modified glass ionomer cements is strontium, which has been associated to a decrease in the amount of acid that S. mutans produces in biological membranes [7].

The phosphate glass leads to the establishment of diverse Zn-O-P linkages, with the incorporation of ZnO will enhance the chemical resilience and longevity of alkali and alkaline of phosphate glasses. Based on the previous study, the improvement in the stability of the glasses could be made by adding the pure SrO to pure phosphate glasses that can form a meta-phosphate structure [9]. In addition, the other study of SrO resulting on how SrO affected the characteristics of the structural of phosphate glasses while the increment of SrO caused the depolymerization of the phosphate network then leading to the decreasing of the connection of the glasses along with the dimensions [10]. While as for the Li_2O as alkali oxides, the introduction of these oxides into oxide glasses leading to de-polymerization then will give in non-bridging oxygen as a result [11].

Derived from cellulose, a naturally occurring polymer found in large quantities in plant cell walls, carboxymethyl cellulose (CMC) has shown promise as a material for the development of sophisticated active and intelligent packaging materials. It is an anionic, water-soluble derivative of cellulose, a linear polysaccharide of anhydro-glucose [8]. CMC has gained popularity as an alternative to packaging materials made of petroleum. Because of its strong polarity, it boosts the mechanical strength, moisture and gas barrier qualities, and crystallinity of starch films while exhibiting cohesive properties [13]. CMC-based composites have gained a lot of recognition for their easy availability, biocompatibility, water solubility, easy structural modifications, and non-toxicity [12].

There have been reports of low water content and effective barrier qualities against oxygen and other fragrance components in edible films made from cellulose derivatives. There are several cellulose derivatives that are known to produce continuous matrixes, like carboxymethyl cellulose (CMC). Since it is easily soluble in water, these cellulose esters pose no health risks to people [12]. It is a mucoadhesive, biocompatible, and biodegradable polymer that forms due to hydrogen bonding. According to recent reports, CMC uses hydrogen bonding to start HA deposition [13]. The production

of self-clean coating materials has seldom ever employed carboxymethyl cellulose (CMC), despite the fact that it is highly beneficial in encouraging the usage of biopolymers. For a variety of uses, it can be enhanced into hydrogels, films, frames, blends, and composites [16]. Then the CMC forming properties can seal the surface, protecting it from contaminants while maintaining self-cleaning functionality. In recent years, several researchers have discovered some fantastic, cutting-edge hybrid polymers with CMC to remove a variety of contaminants from wastewater. According to a recent research, CMCs are an inexpensive binder for biomass pellets that significantly improved the pellets' quality, durability, and compressive strength while lowering the energy consumption of the shells [8].

However, the number of studies concerned with the structural and mechanical properties of the glass-forming region P_2O_5-ZnO-Li_2O-SrO glass containing carboxymethyl cellulose has been limited and not well investigated. The purpose of this study is to investigate how the optimal dopant concentrations and structural and mechanical properties of carboxymethyl cellulose doped into phosphate glass systems are affected and able to maintain the surface that are clean. The self-cleaning effect ensures that microplastics are easily removed with water, preventing contamination in critical environments.

This study investigates the influence of CMC doping on phosphate glasses with the composition (40–x) P_2O_5-ZnO-Li_2O–SrO-xCH_2CO_2H ($0.0 \leq x \leq 0.5$ mol%). The goal is to understand the role of CMC in enhancing the glass network and its potential to develop self-cleaning, non-toxic surfaces for critical environments such as food processing and healthcare. By characterizing the structural and mechanical changes induced by CMC, this research aims to contribute to the development of innovative, biodegradable materials for sustainable applications.

2. Methodology

The glass sample with composition of (40–x) P_2O_5-ZnO-Li_2O-SrO-*x*CH_2CO_2H where ($0 \leq x \leq 0.5$ mol%) was prepared by melt quenching technique. The glass composition was prepared in powder form with a mass of 10 g. It begins with the selection of raw materials, which are phosphate pentoxide (P_2O_5), lithium oxide (Li_2O), zinc oxide (ZnO), strontium carbonate (SrO), and carboxymethyl cellulose (CH_2CO_2H) which are weighed using an electronic weighing scale.

Firstly, the glass samples were labeled as S1, S2, S3, S4, S5, and S6 as shown in Table 1. Then, all the materials except phosphate pentoxide (P_2O_5) will be put in a plastic bottle. Then, all the materials except phosphate pentoxide (P_2O_5) will be put in a plastic bottle. The weighed material was put in the milling machine for 30 minutes to get a homogeneous mixture. Then, the homogeneous mixture was put in an alumina crucible, including the phosphate pentoxide (P_2O_5) and put in the furnace to be pre-heated with a temperature of 300°C for one hour to remove moisture from the mixture.

Then, it was transferred to another furnace with a temperature of 1000 °C for 30 minutes for the mixture to melt. The molten material was then poured on a metal plate that was heated in a furnace at 300 °C temperature and the annealing process took 3 hours at 300 °C to remove any remaining tensions from the glass. This procedure was repeated for all glass samples with varied mol% concentrations, as shown in Table 1.

Table 1
The composition of (40–x) P_2O_5-ZnO-Li_2O-SrO-$x CH_2CO_2H$ where (0 ≤ x ≤ 0.5 mol%)

Samples	Composition (mol%)				
	P_2O_5	ZnO	Li_2O	SrO	CH_2CO_2H
S1	40.0	30	25	5	0.0
S2	39.0	30	25	5	0.1
S3	39.8	30	25	5	0.2
S4	39.7	30	25	5	0.3
S5	39.6	30	25	5	0.4
S6	39.5	30	25	5	0.5

FTIR is a technique that is used to identify a molecule's chemical bonds by generating an infrared absorption spectrum. The background spectra of FTIR were first set up in the computer, and the spectra of samples is recorded in the wavenumber range of 4000-650 cm^{-1} with resolutions of 4 cm^{-1} by using an Attenuated Total Reflectance (ATR) system and analysed with the Perkin Elmer FTIR Spectrometer Frontier GP0B version. FTIR are able to detect the internal molecular structures due to the chemical bonds and functional groups that are formed by atoms are in constant vibration states involving bridging and non-bridging oxygens. The technique allows the characterization of specific on this phosphorus containing molecular structures. The software Origin Pro 2022 was then used to analyse and the raw data is plotted. While FTIR provides detailed qualitative information about molecular structures, quantifying the concentration of specific components is less precise without additional calibration. The other complementary characterization techniques like Raman spectroscopy being used for comprehensive molecular and structural analysis.

Raman spectroscopy is where the sample's vibrational energy modes are measured using scattered light. It is used to determine the change in structural around the phosphate atom in a glass sample. A Micro Raman Mapping System Model: Unidron-A (2019) was used to make the Raman measurement, with an acquisition time of 10s and a spectral range of 4000 - 100 cm^{-1} in wavenumber. To get the right position of the sample and a clear image on the window, the stage can be adjusted by controlling the control knob. For analysis, Raman offering a quick characterization then provides detailed information about structure and composition of bio-molecules due to its non-invasive nature which are very suitable to be used in this study to detect any changes in phosphate network connectivity upon the addition of CMC to understand better about the self-cleaning mechanism.

A micro-indentation method is the Vickers hardness test, often known as the 136° diamond pyramid hardness test. The diagonals of the square indentation that the indenter creates are measured. The Vickers hardness testing machine directly provides the Vickers hardness number (VHN). The Vickers hardness measurements were performed in air at room temperature under a constant loading. Using an indenter and 200 g of force, the specimen's surface was initially indented in that machine for a dwell period of 20 seconds. On every specimen, the hardness was tested at three different locations. The most suitable value among the three values was determined for this assessment.

The mechanical properties of glass samples were characterized by ultrasonic testing by Pulse Echo Method. The waveform analysis yielded the three fundamental parameters: frequency, amplitude, and time of flight. The thickness of the bulk glass samples was measured using a vernier calliper and before ultrasonic scanning, essential oil was applied to the surface of the scan area of the sample as well as the ultrasonic probe before ultrasonic scanning. This is to make sure that there will be no reflection during the transfer of ultrasonic waves to the sample due to the air gap between them. The refraction angle of 45° of the angle wedges made from Perspex was used. The pulse oscillator's output was dependent upon the transmitting transducer's ability to convert it into an acoustic pulse. Following their generation through the glass sample, these pulses were received by the transducer

and transformed into electric signals. Thus, the output signal (amplified) from the sample is displayed on the oscilloscope. The information obtained was taken for the calculation of elastic constant measurements, which can be evaluated by using the equations obtained from the literature.

3. Results

A series of glasses with the composition of (40–x) P_2O_5-ZnO-Li_2O-SrO-*x*CH_2CO_2H where (0 ≤ x ≤ 0.5 mol%) for 10 g have successfully been prepared by using conventional melt-quenching techniques were shown in Figure 1. The physical characteristics of each glass, which vary in composition concentration, as glassy and transparent, were tabulated in Table 2.

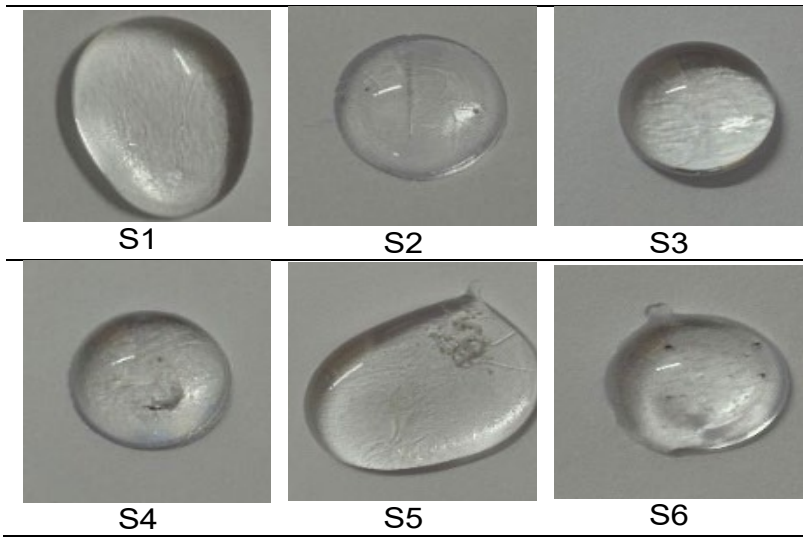

Fig. 1. Glass of (40 – x) P_2O_5–ZnO-Li_2O–SrO-*x*CH_2CO_2H

Table 2
The composition of (40–x) P_2O_5-ZnO- Li_2O-SrO-*x*CH_2CO_2H where (0 ≤ x ≤ 0.5 mol%)

Samples	Composition (mol%)					Appearances
	P_2O_5	ZnO	Li_2O	SrO	CH_2CO_2H	
S1	40.0	30	25	5	0.0	Colorless and transparent
S2	39.9	30	25	5	0.1	Colorless and transparent
S3	39.8	30	25	5	0.2	Colorless and transparent
S4	39.7	30	25	5	0.3	Colorless and transparent
S5	39.6	30	25	5	0.4	Colorless and transparent
S6	39.5	30	25	5	0.5	Colorless and transparent

Using FTIR-ATR, the corresponding phosphate glass was measured. The structural characteristics of the samples in terms of functional group and fundamental were determined by analysing the IR. At room temperature, the glasses' IR absorption spectra were observed within the 4000-650 cm^{-1} range. Figure 2 displays the ATR-FTIR spectra of (40–*x*) P_2O_5–ZnO-Li_2O–SrO-*x*CH_2CO_2H where (0.0 ≤ x ≤ 0.5 mol%) and it has seven absorption bands. Every band corresponds to a specific functional group's vibration. Table 3 shows the FTIR peak positions of the glass system for each sample, and

Table 4 shows the suggested assignment included a summary of the positions of the absorption peaks.

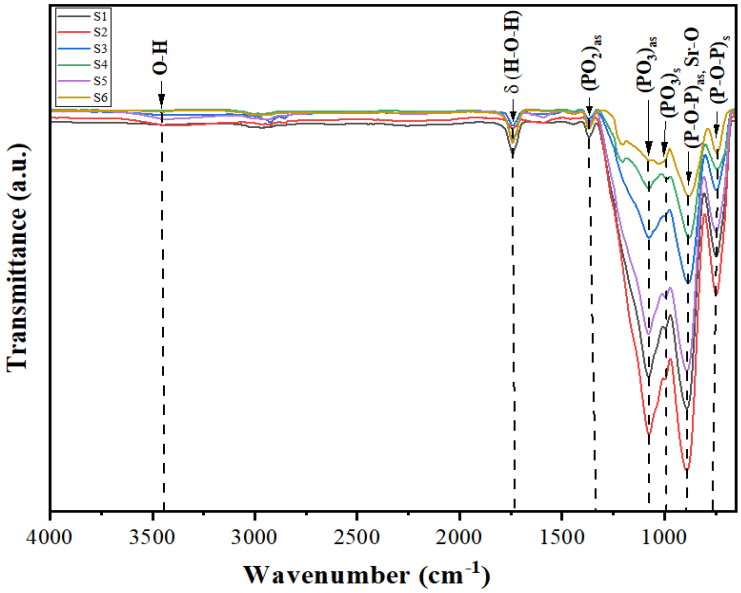

Fig. 2. FTIR spectra of (40 – *x*) P_2O_5-ZnO-Li_2O-SrO-*x*CH_2CO_2H where (0 ≤ x ≤ 0.5 mol%) glass system

Table 3
The FTIR peaks positions of the glass system

Sample	IR Band (cm^{-1})						
1	752	886	993	1077	1368	1745	3453
2	753	897	995	1077	1368	1740	3453
3	750	890	998	1080	1370	1740	3454
4	734	881	995	1079	1367	1741	3451
5	744	888	994	1077	1375	1740	3456
6	736	886	996	1073	1372	1744	3451

Table 4
Band position of FTIR spectra of the glass system

No	IR Band (± 0.1 cm^{-1})	Assignments	References
1	736 – 753	Assign as P-O-P bridges and is a symmetric stretching vibration, v_s (P-O-P)	(Algradee *et al.,* 2022), (Mao *et al.,* 2023), (Radouane *et al.,* 2020)
2	881 – 890	Assign as P-O-P bridges and is an asymmetric stretching, v_{as} (P-O-P), Sr – O stretching	(Farag *et al.,* 2022), (Alimuddin & Rafeeq, 2021)
3	993 – 998	Symmetric stretching band, (P-O-P) of PO_3, v_s (P-O-P)	(Algradee *et al.,* 2022)
4	1073 – 1080	Asymmetric stretching band, (P-O-P) of PO_3, v_{as} (P-O-P)	(Azmi *et al.,* 2015), (Farag *et al.,* 2022)
5	1368 – 1375	Asymmetric stretching band, (P-O-P) of PO_2, v_{as} (P-O-P)	(Ibrahim *et al.,* 2024)
6	1740 - 1745	H – O – H bending vibration	(Narsimha *et al.,* 2023)
7	3451 - 3456	Fundamental stretching of O-H groups	(Abdelghany *et al.,* 2018), (Algradee *et al.,* 2022), (Adibah., 2023)

It is generally known that glass modification oxides can affect glass structure by changing bridging oxygen into non-bridging oxygen, which depolymerizes the glass network structure. There is a substantial correlation between the oxygen/phosphate (O/P) ratio in glass compositions and the structure of phosphate glasses. Phosphate networks depolymerize more as the O/P ratio rises. This means that a phosphate structure made of cross-linked Q^3 units becomes a chain-like metaphosphate structure composed of Q^2 units, a pyrophosphate structure composed of Q^1, and finally an orthophosphate structure made up of isolated Q^0 units. The pyrophosphate (Q^1) and orthophosphate (Q^0) groups have low leaching rates in water and outstanding chemical durability, but the metaphosphate (Q^2) group has a terrible one [17].

Raman spectroscopy is used to determine the presence of distinct structural units and the structural unit modifications that arise from the addition of modifier ions. Its outcome is an addition to FTIR spectra. Raman scattering's inelastic energy range is comparatively smaller than vibrational energy, where the wave number range is considered from 200 to 1300 cm^{-1}. Figure 3 represents the Raman spectra of the prepared glass sample. Table 5 list the Raman shifts, and Table 6 represents the seven identified spectral regions.

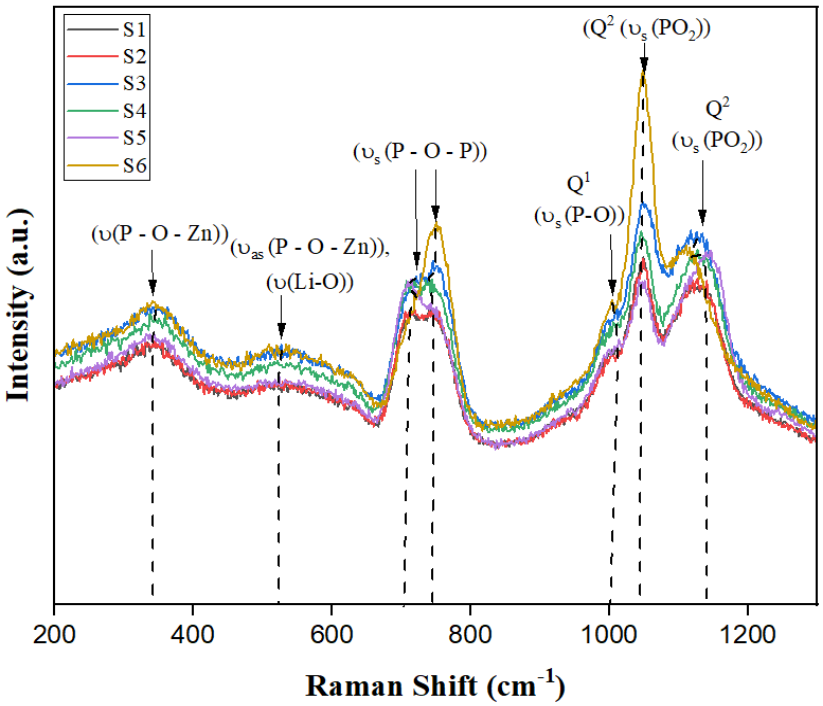

Fig. 3. Raman shift spectra of (40 – *x*) P_2O_5-ZnO-Li_2O-SrO-*x*CH_2CO_2H where (0 ≤ *x* ≤ 0.5 mol%) glass system

Table 5
Raman shift position of (40 – *x*) P_2O_5-ZnO-Li_2O-SrO-*x*CH_2CO_2H where (0 ≤ *x* ≤ 0.5 mol%) glass system

Sample	Raman Shifts (cm-1)						
	(δ(P-O-Zn))	(δ_{as}(P-O))	$\boldsymbol{\upsilon_s}$ (P-O-P)	$\boldsymbol{\upsilon_s}$ (P-O-P)	Q^1 ($\boldsymbol{\upsilon_s}$ (P-O))	Q^2 ($\boldsymbol{\upsilon_s}$ (PO_2))	Q^2 ($\boldsymbol{\upsilon_s}$ (PO_2))
1	341	527	714	740	1012	1049	1135
2	342	527	719	744	1012	1045	1140
3	342	529	721	745	1010	1047	1140
4	344	527	714	744	1012	1045	1142
5	342	525	714	742	1014	1042	1147
6	342	530	714	749	1004	1049	1120

Table 6
Raman shift of (40 – *x*) P_2O_5-ZnO-Li_2O-SrO-*x*CH_2CO_2H where (0 ≤ x ≤ 0.5 mol %) glass system

No.	Raman Shifts (cm^{-1})	Assignments	References
1	341 – 344	Bending vibration of P – O – Zn	(Yusof *et al.,* 2022)
2	525 – 530	P-O bonds exhibiting asymmetric bending vibrations in P^1 and P^2 tetrahedra, Sr – O stretching	(Ahlawat *et al.,* 2024), (Y. G. Zhu *et al.,* 2022
3	714 – 719	Symmetric stretching mode of P-O-P bridge, υ_s (P-O-P)	(Azmi *et al.,* 2015)
4	740 – 749	Symmetric stretching mode of P-O-P bridge, υ_s (P-O-P)	(Chahine *et al.,* 2004)
5	1004 – 1014	Symmetric stretching mode of P-O in Q^1	(Brow *et al.,* 1995)
6	1042 – 1049	Symmetric stretching mode of $(PO_2)^-$ vibration, υ_s (PO_2) in Q^2 unit	(Adibah., 2023)
7	1120 – 1147	Symmetric stretching mode of $(PO_2)^-$ vibration, υ_s (PO_2) in Q^2 unit	(Jlassi *et al.,* 2022), (Goj *et al.,* 2022)

The P-O-P bridge's symmetric stretch is what causes the vibration at the second sharp peak at 740-749 cm^{-1}. The band position about 1004-1014 cm^{-1} was approved for Symmetric stretching mode of P-O in Q1. The vibrations at 1042-1049 cm^{-1} and 1120-1147 cm^{-1} are associated with the non-bridging oxygens (PO_2) symmetric stretching mode, noted υs (PO_2) in Q^2 unit [18]. Moreover, the vibrational peak cannot arise in the presence of CMC at comparatively higher doping levels, indicating that the CMC are uniformly distributed throughout the material without clumping together.

The host lattice vibrational is not affected by CMC because its concentration in the glass system is less than 1%, which is between 0 and 0.5 mol%. Consequently, it may be said that the emergence of bridging oxygen causes the band to move to a higher wave number as the CMC concentration rises. The phosphate group depolymerization, which changed with the addition of CMC content, was clearly described by the analysis above. hence supporting the FTIR results as well.

To determine the elastic properties produced by a small stress, ultrasonic measurement was used. It can provide both longitudinal and shear elastic constants of all glasses, as shown in Table 7. Figure 4 represents the ultrasonic longitudinal and shear wave velocities against CMC concentration (%mol). This study aims to use the pulse echo technique to evaluate the longitudinal and ultrasonic velocities of glass samples and to determine their mechanical properties. The measurement of Young's modulus (E), bulk modulus (K), microhardness (H), and Poisson's ratio (σ) can also be determined using the sound velocities.

Table 7
The longitudinal and shear velocities with different CMC composition

Mol % of CH_2CO_2H	Longitudinal Velocity, V_L (ms^{-1})	Shear Velocity, V_S (ms^{-1})
0.0	5242.60	3642.42
0.1	5379.31	4489.31
0.2	6653.59	5016.27
0.3	5292.31	4490.67
0.4	5139.90	4078.20
0.5	5112.43	3993.07

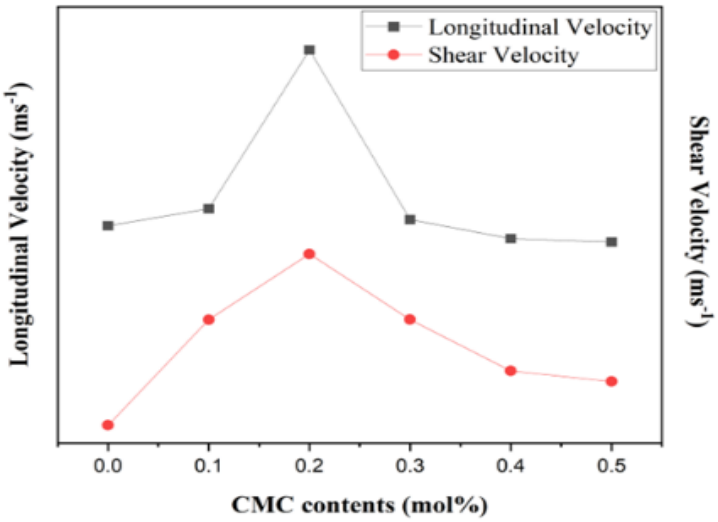

Fig. 4. Ultrasonic longitudinal and shear wave velocities against CMC concentration (mol%)

The glass system indicated in Table 8 is found to have an impact on the ultrasonic velocities measured from the samples. Tables 8 and 9 show that as CMC increased, all of the elastic moduli values fell. Shear modulus experiences this nonlinear change as well, following the same general pattern. In terms of Young's modulus, *E*, it has the same trend as the bulk modulus, *K*, which is likewise identical. Figure 5 shows the variation of elastic moduli with different mol% of CMC, and Figure 6 shows microhardness, H of composition (40 – *x*) P_2O_5-ZnO-Li_2O-SrO-*x*CH_2CO_2H where (0 ≤ *x* ≤ 0.5 mol%) glass system.

Table 8
Variation of elastic moduli and Poisson's ratio with addition of CMC

Mol % of CH_2CO_2H	Longitudinal Modulus, *L* (GPa)	Shear Modulus, *G* (GPa)	Bulk Modulus, *K* (GPa)	Young's Modulus, *E* (GPa)	Poisson's Ratio, σ
0.0	71.57	71.57	19.96	70.53	-0.09
0.1	79.69	79.69	5.68	39.15	-0.65
0.2	141.40	80.37	34.24	135.27	-0.16
0.3	88.70	63.87	3.55	27.37	-0.79
0.4	81.13	51.08	13.03	66.43	-0.35
0.5	73.18	44.64	13.66	64.09	-0.28

Table 9
Poisson's ratio (σ) and Microhardness, H of glass structure with different CMC contents

Mol % of CH_2CO_2H	Poisson's Ratio, σ	Microhardness, *H* (GPa)
0.0	-0.09	15.19
0.1	-0.65	42.45
0.2	-0.16	35.28
0.3	-0.79	54.74
0.4	-0.35	28.93
0.5	-0.28	23.28

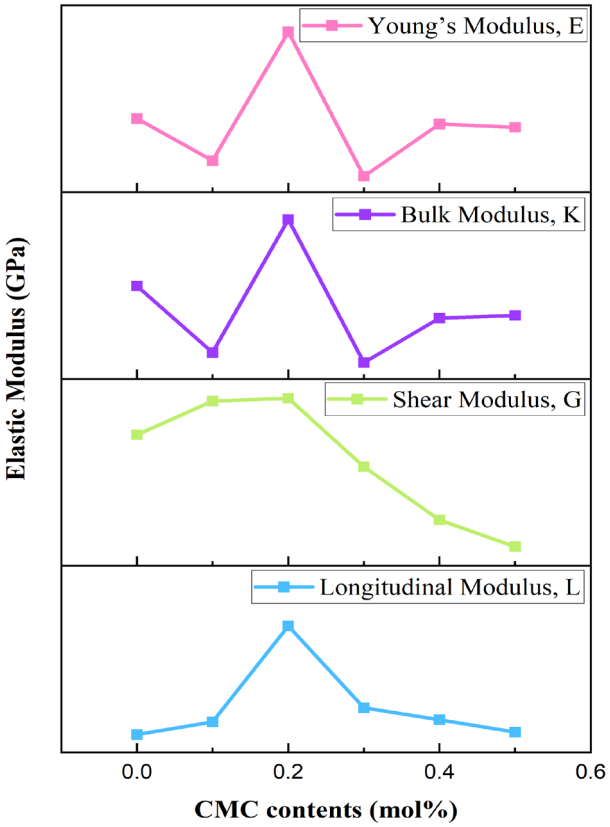

Fig. 5. The variation of elastic moduli with different mol% of CMC

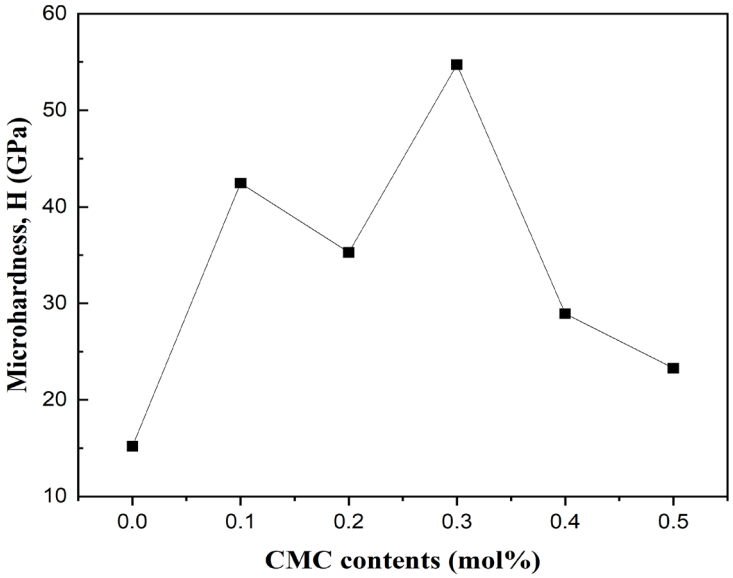

Fig. 6. Microhardness, H of composition (40 – *x*) P_2O_5-ZnO-Li_2O-SrO-*x*CH_2CO_2H where ($0 \leq x \leq 0.5$ mol%) glass system

The decrease in the σ value with increasing CMC concentration could potentially be explained to an increase in glass ionicity caused by increased polar bonding inside the modifiers [19]. Figure 7 shows the decreasing of Poisson's ratio pattern trend suggests a weakening of the glass system network, which in turn shows a decrease in glass stiffness.

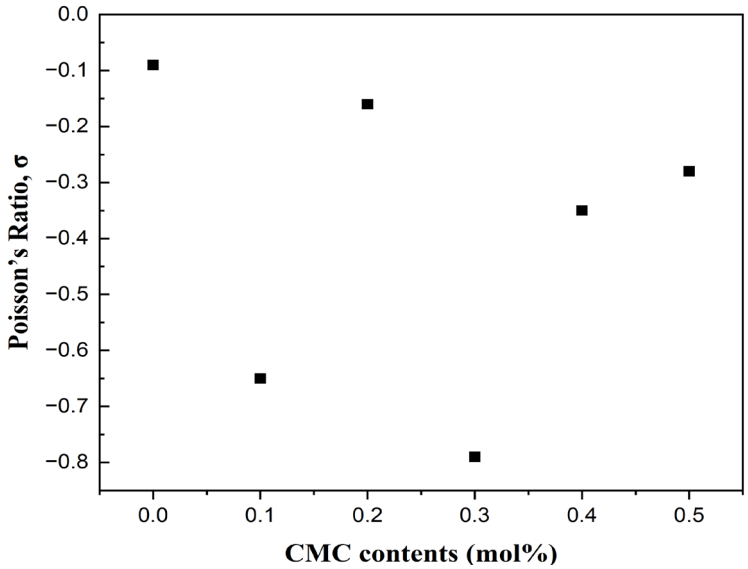

Fig. 7. Poisson's ratio, σ of composition (40 – *x*) P_2O_5-ZnO-Li_2O-SrO-*x*CH_2CO_2H where (0 ≤ *x* ≤ 0.5 mol%) glass system

The mechanical properties are obtained from data of Vickers hardness (H_v) testing and calculations of fracture toughness (K_{Ic}) and brittleness (B), as shown in Table 10, Table 11, and Table 12. The rise in the molecular weight of the host glass causes an increase in the density values of glass samples but decreases in H_v when the concentration of CMC increases. In glass matrices, the decrease in bond length causes a drop in molecular volume [20]. Figure 8 below shows the Vickers hardness with a variation of CMC.

Table 10
The values of the Vickers hardness, H_v of glass sample

Sample	Vickers hardness, H_v (GPa)	References
1	3.86	Present research
2	4.08	Present research
3	4.14	Present research
4	4.11	Present research
5	4.10	Present research
6	4.09	Present research
$20Li_2O - 80P_2O_5$	4.55	(Salama & El-Batal, 1994)
$40P_2O_5$-30ZnO-$25Li_2O$-5SrO	4.51	(Nur Ain., 2024)

Table 11
The fracture toughness (K_{Ic}) of glass sample

Sample	K_{Ic} (GPamm$^{1/2}$)	References
1	0.0069	Present research
2	0.0138	Present research
3	0.0128	Present research
4	0.0079	Present research
5	0.0189	Present research
6	0.0173	Present research
50BaO–$50P_2O_5$-$4Ag_2O$–4SnO	0.2600 – 0.2810	(Narayanan & Shashikala, 2016)

Table 12
The comparison of present and previous research of brittleness (B) of glass samples

Sample	B ($mm^{-1/2}$)	References
1	559.01	Present research
2	296.46	Present research
3	323.82	Present research
4	518.86	Present research
5	216.54	Present research
6	236.89	Present research
$50BaO – 50P_2O_5 – 4Ag_2O – 4SnO$	1132.00 – 1099.00	(Narayanan & Shashikala, 2016)
$39P_2O_5$ - 30ZnO -$25Li_2O$ - 5SrO - CS	504.31	(Nur Ain., 2024)

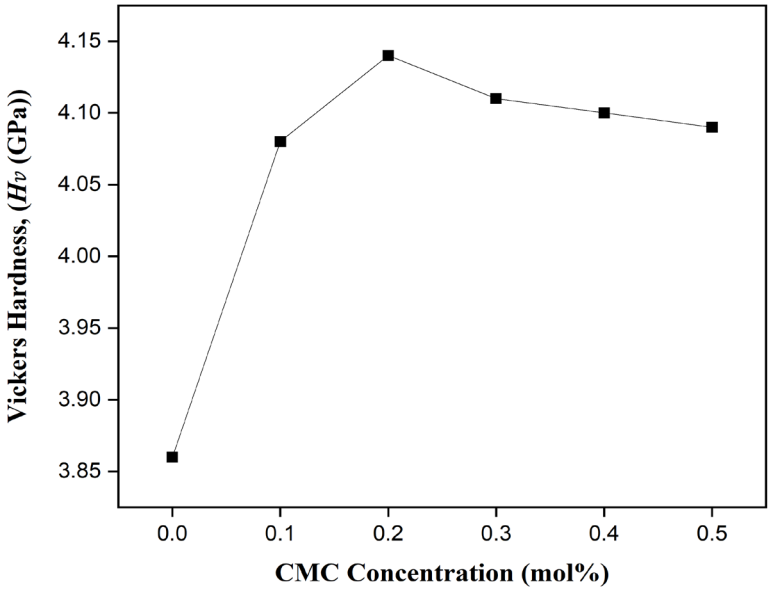

Fig. 8. The Vickers hardness with a variation of CMC

The rise in the molecular weight of the host glass causes an increase in the density values of glass samples when the concentration of CMC increases. In glass matrices, the decrease in bond length causes a drop in molecular volume. The bond strength between CMC ions and oxygen increases as the improved compactness of CMC concentration grows, and this is because of an increase in field strength [20]. According to popular belief, the type and strength of the bonds determine the H_v.

Depending on the concentration of CMC added, the glass's K_{Ic} can either increase or decrease. Compressive stress is encountered when Hv generates a radial-median crack. When the fracture front reaches a critical penetration depth, it overcomes the trapping effect and begins to propagate once more between the particles. This lessens the propagation of cracks through the compressive stress-filled glass. Thus, when glass contains compressed and strained metal particles embedded in it, thermal residual stresses enhance the mechanical properties of the glass. Figure 9 shows the fracture toughness, K_{Ic} with the variation of CMC.

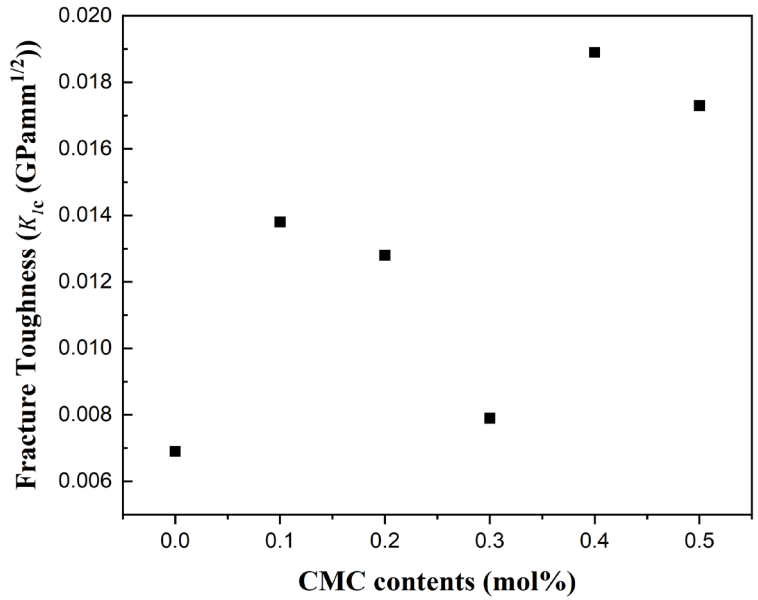

Fig. 9. The fracture toughness, K_{Ic} with the variation of CMC

Based on Figure 10, it is observed that the pattern of brittleness B is inversely proportional to the fracture toughness, K_{Ic}. A proportional drop in the value of B occurs with an increase in CMC. The study's findings showed that glass has gotten harder.

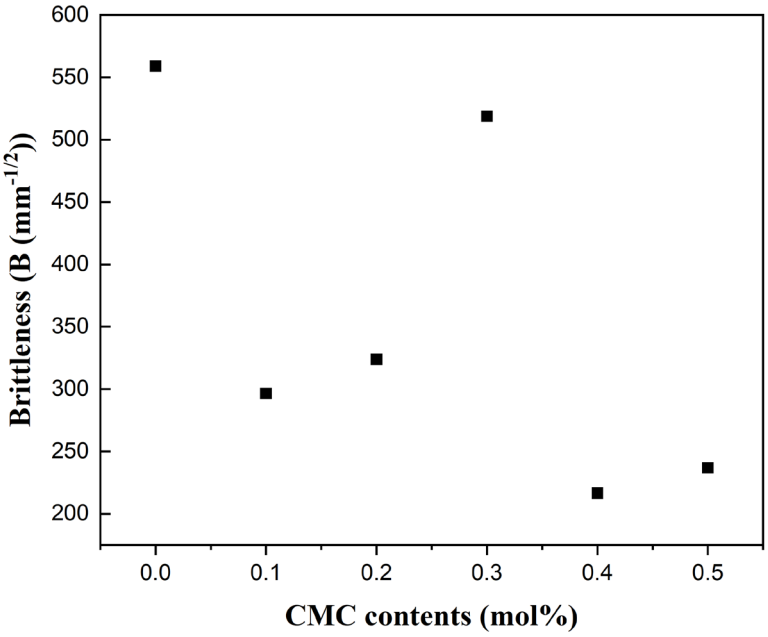

Fig. 10. The brittleness, B with the variation of CMC

4. Conclusions

This study examined the impact of carboxymethyl cellulose (CMC) doping on the structural and mechanical properties of phosphate glasses. The incorporation of CMC into the (40–x) P_2O_5-ZnO-Li_2O–SrO-xCH_2CO_2H system resulted in notable improvements in stiffness, compactness, and self-cleaning properties, with the glass maintaining a uniform structure even at higher doping levels. FTIR

and Raman spectroscopy confirmed changes in the phosphate network, while mechanical testing demonstrated enhancements in hardness and elasticity.

These findings underscore the potential of CMC-doped phosphate glasses for applications in industries where contamination prevention and sustainability are priorities, such as food processing and healthcare. The biodegradable and non-toxic nature of these materials offers an environmentally friendly alternative to conventional synthetic coatings. Future research could focus on optimizing the glass composition for specific applications, scaling up production, and evaluating performance under real-world conditions. This work lays the foundation for innovative, sustainable solutions in glass technology.

Acknowledgement
The authors express gratitude to the Research Management Centre (RMC) and the Ministry of Higher Education Malaysia (MoHE) for financial support through the Fundamental Research Grant Scheme (FRGS) vot number R.J130000.7854.5F635 (PY/2023/02164) and International Grant Nippon Sheet Grant (NSG) vot number R.J130000.7354.4B743 (PY/2021/02736). The authors also would like to acknowledge the financial support: University Industry Research Lab (UIRL), PPMU, UTM under Dana Universiti Penyelidikan (Caj Analisis Makmal) - Q.J091600.3100.00A37. The authors also gratefully acknowledge their colleagues at Universiti Teknologi Malaysia especially members of the Advanced Optical Materials Research Group (AOMRG).

References

[1] Karbalaei, Samaneh, Abolfazl Golieskardi, Hazilawati Binti Hamzah, Samiaa Abdulwahid, Parichehr Hanachi, Tony R. Walker, and Ali Karami. "Abundance and characteristics of microplastics in commercial marine fish from Malaysia." *Marine pollution bulletin* 148 (2019): 5-15. https://doi.org/10.1016/j.marpolbul.2019.07.072

[2] Patidar, Kalpana, Mohammed Alshehri, Wrick Singha, Muneera Alrasheedi, Alaa M. Younis, Umesh Chandra Dumka, and Balram Ambade. "Assessing the microplastic pandemic: Prevalence, detection, and human health impacts in Asian aquatic environments." *Physics and Chemistry of the Earth, Parts A/B/C* (2024): 103800. https://doi.org/10.1016/j.pce.2024.103800

[3] Kumar, MB Sunil, and B. Eraiah. "Effect gamma irradiation on structural properties of lithium zinc phosphate glass doped with MoO3." *Nuclear and Particle Physics Proceedings* 341 (2023): 34-38. https://doi.org/10.1016/j.nuclphysbps.2023.09.014

[4] Shaaban, Kh S., El Sayed Yousef, Safwat A. Mahmoud, EA Abdel Wahab, and E. R. Shaaban. "Mechanical, structural and crystallization properties in titanate doped phosphate glasses." *Journal of Inorganic and Organometallic Polymers and Materials* 30 (2020): 4655-4663. https://doi.org/10.1007/s10904-020-01574-x

[5] Lee, Myung-Jin, Young-Bin Seo, Ji-Young Seo, Jeong-Hyun Ryu, Hyo-Ju Ahn, Kwang-Mahn Kim, Jae-Sung Kwon, and Sung-Hwan Choi. "Development of a bioactive flowable resin composite containing a zinc-doped phosphate-based glass." *Nanomaterials* 10, no. 11 (2020): 2311. https://doi.org/10.3390/nano10112311

[6] Singh, Gurinder Pal, Joga Singh, Parvinder Kaur, Simranpreet Kaur, Deepawali Arora, Ravneet Kaur, and D. Pal Singh. "Comparison of structural, physical and optical properties of Na2O-B2O3 and Li2O-B2O3 glasses to find an advantageous host for CeO2 based optical and photonic applications." *Journal of Non-Crystalline Solids* 546 (2020): 120268. https://doi.org/10.1016/j.jnoncrysol.2020.120268

[7] Go, Hye-Bin, Myung-Jin Lee, Ji-Young Seo, Sung-Yun Byun, and Jae-Sung Kwon. "Mechanical properties and sustainable bacterial resistance effect of strontium-modified phosphate-based glass microfiller in dental composite resins." *Scientific reports* 13, no. 1 (2023): 17763. https://doi.org/10.1038/s41598-023-44490-z

[8] Rahman, Md Saifur, Md Saif Hasan, Ashis Sutradhar Nitai, Sunghyun Nam, Aneek Krishna Karmakar, Md Shameem Ahsan, Muhammad JA Shiddiky, and Mohammad Boshir Ahmed. "Recent developments of carboxymethyl cellulose." *Polymers* 13, no. 8 (2021): 1345. https://doi.org/10.3390/polym13081345

[9] Han, Lei, Qian Zhang, Jun Song, Zongliang Xiao, Yaochun Qiang, Xinyu Ye, Weixiong You, and Anxian Lu. "A novel Eu3+-doped phosphate glass for reddish orange emission: Preparation, structure and fluorescence properties." *Journal of Luminescence* 221 (2020): 117041. https://doi.org/10.1016/j.jlumin.2020.117041

[10] El Jouad, Mohamed, Samira Touhtouh, and Abdelowahed Hajjaji. "First investigation of the effect of strontium oxide on the structure of phosphate glasses using molecular dynamics simulations." *Computational Materials Science* 220 (2023): 112068. https://doi.org/10.1016/j.commatsci.2023.112068
[11] Ahlawat, Jyoti, Suman Pawaria, Anil Ohlan, Sajjan Dahiya, Rajesh Punia, and A. S. Maan. "Correlation between Structural and Optical Characterizations of IR transparent Sodium Modified Zinc Phosphate Oxide Glasses." *Journal of Molecular Structure* (2024): 138794. https://doi.org/10.1016/j.molstruc.2024.138794
[12] Tyagi, Vishal, and Archana Thakur. "Applications of biodegradable carboxymethyl cellulose-based composites." *Results in Materials* (2023): 100481. https://doi.org/10.1016/j.rinma.2023.100481
[13] Adhikary, Nibedita Das, Aarti Bains, Mansuri M. Tosif, Prince Chawla, Nemat Ali, Mushtaq Ahmad Ansari, Sanju Bala Dhull, and Gulden Goksen. "Development of ternary polymeric film based on modified mango seed kernel starch, carboxymethyl cellulose, and gum acacia to extend the shelf-life of bun-bread." *International Journal of Biological Macromolecules* (2024): 132915. https://doi.org/10.1016/j.ijbiomac.2024.132915
[14] Mukherjee, Sohini, Avery Sengupta, Subham Preetam, Tanmoy Das, Tanima Bhattacharya, and Nanasaheb Thorat. "Effects of fatty acid esters on mechanical, thermal, microbial, and moisture barrier properties of carboxymethyl cellulose-based edible films." *Carbohydrate Polymer Technologies and Applications* 7 (2024): 100505. https://doi.org/10.1016/j.carpta.2024.100505
[15] Güben, Esra, Ergün Bozdağ, and Duygu Ege. "Preparation of calcium phosphate/carboxymethylcellulose-based bone cements." *Bioinspired, Biomimetic and Nanobiomaterials* 9, no. 3 (2020): 155-163. https://doi.org/10.1680/jbibn.19.00053
[16] Revathi, S., Mohammed Amanullah, Awad Saeed Al-Samghan, J. John Joseph, P. Pazhanisamy, Mourad Addich, and Thandapani Gomathi. "Sustainable heavy metal (cr (vi) ion) remediation: Ternary blend approach with chitosan, carboxymethyl cellulose, and bioactive glass." *International Journal of Biological Macromolecules* 278 (2024): 134769. https://doi.org/10.1016/j.ijbiomac.2024.134769
[17] Lu, Mingwei, Fu Wang, Qilong Liao, Kuiru Chen, Jianfa Qin, and Sheqi Pan. "FTIR spectra and thermal properties of TiO2-doped iron phosphate glasses." *Journal of Molecular Structure* 1081 (2015): 187-192. https://doi.org/10.1016/j.molstruc.2014.10.029
[18] Goj, Pawel, Aleksandra Wajda, Pawel Stoch, and Barbara Marczewska. "Raman spectroscopy of β-irradiated aluminum-iron phosphate glass." *Journal of Molecular Structure* 1258 (2022): 132605. https://doi.org/10.1016/j.molstruc.2022.132605
[19] Algradee, Mohammed A., Emran Eisa Saleh, O. M. Samir, A. B. Alwany, and Tharwat M. EL Sherbini. "Evaluation of structural, elastic properties and nuclear radiation shielding competence of Nd3+ doped lithium-zinc-phosphate glasses." *Journal of Non-Crystalline Solids* 576 (2022): 121304. https://doi.org/10.1016/j.jnoncrysol.2021.121304
[20] Kumar, MB Sunil, and B. Eraiah. "Physical and structural properties of molybdenum doped lithium zinc phosphate glass." Materials Today: Proceedings 92 (2023): 1310-1318. https://doi.org/10.1016/j.matpr.2023.05.490